

Amorphous and Microcrystalline Silicon-based Photovoltaic

Subhendu Guha
United Solar Ovonic Corporation
3800 Lapeer Road
Auburn Hills, MI 48326, U.S.A.

ABSTRACT

The last two decades have witnessed tremendous progress in the science and technology of amorphous and microcrystalline silicon-based photovoltaic. Advances in the understanding of materials and devices have led manufacturers to expand their production capacity; the production of solar panels based on this technology exceeded 25 MW in 2003. Hydrogen dilution in the active gas mixture during deposition has played a key role in improving the quality of the materials and the performance of the devices. In this paper I shall review the properties of the optimum material for device application, and discuss the production status. I shall also report on the new opportunities that are opening up for these products for space and stratospheric applications.

INTRODUCTION

Significant progress has been made in the field of science and technology of amorphous silicon (a-Si) alloys in the last two decades. When the first MRS symposium on a-Si alloy took place in 1985, the focus rightfully was on material aspects. Our understanding of multi-junction devices was at its infancy; manufacturing also was in very small volume for consumer products only. The field has matured significantly with contribution from a very active international scientific community; the industry is also thriving with production in 2003 exceeding 25 MW with the products used in applications ranging from battery charging for small appliances to large-scale grid-connected systems. While the industrial focus has been mainly on multi-junction cells using a-Si and amorphous silicon germanium (a-SiGe) alloys [1], research on microcrystalline silicon has established it as a potential material for use in the bottom cells of such devices [2].

a-Si alloy is usually prepared by glow-discharge decomposition of silane. It was first shown by Guha et al. [3] that superior film properties could be obtained by using a dilute mixture of silane in hydrogen. As the hydrogen dilution is increased, the transition from amorphous to microcrystalline phase takes place. Recent work has shown that the best amorphous silicon is grown at a dilution just below the edge of amorphous to microcrystalline transition [4]. On the other hand, the highest efficiency microcrystalline solar cells are made when the hydrogen dilution pushes the material just above the edge [5]. The material near the edge thus has received a great deal of attention. In this paper, we discuss material and cell properties of thin-film silicon in this deposition regime. We shall also describe the manufacturing technology of solar cells using this material, and some new applications.

MATERIAL BELOW THE EDGE (AMORPHOUS PHASE)

Plasma Chemistry

The basic plasma chemistry prevalent in a discharge of silane with or without hydrogen dilution has been investigated extensively [6,7]. Electron-molecule collisions dissociate the molecules into ions and neutral radicals. These radicals undergo various secondary reactions during their transport to the substrate. Of the various species (SiH, SiH₂, SiH₃, Si_xH_y etc.) in the plasma, SiH₃ has the longest lifetime. Bonding of SiH₃ to the growing surface needs dangling bonds, and removal of hydrogen from the surface is a necessary step in the deposition of films from SiH₃. Hydrogen can be released from the surface by thermal excitation, or it can be stripped by SiH₃ reacting with SiH to form a dangling bond and silane. Another SiH₃ molecule migrating along the surface or arriving directly can then be incorporated in the film leading to growth.

What is the role of excess hydrogen in the plasma? It provides improved surface coverage that results in the impinging molecules diffusing further to find more energetically favorable sites [8]. Hydrogen dilution should, therefore, result in a more ordered structure; in fact, with increasing hydrogen dilution, one should expect growth of microcrystallites. This has been known for a long time. Hydrogen is also an etchant. During the deposition process, both ordered and disordered regions may be deposited simultaneously, and hydrogen etches away the disordered regions more effectively leaving behind the ordered structure [9]. An alternative explanation for obtaining a more ordered structure with hydrogen dilution is the phenomenon of chemical annealing [10]. This model postulates a structural relaxation of the amorphous phase and transition to crystalline phase by permeation of hydrogen atoms to a sub-surface region. It has been recently demonstrated that atomic hydrogen can be inserted into strained Si-Si bonds in the sub-surface region through the formation of a SiH_n complex. Subsequent structural relaxation of these bonds results in the growth of a more ordered phase. Molecular dynamics simulations also support this model [11].

Structure

The first systematic investigation of the effect of hydrogen dilution on the structure of a-Si alloys was carried out by Tsu et al. [4] using high-resolution transmission electron microscopy (TEM) and Raman spectroscopy. The TEM results showed that embedded in the amorphous matrix are chain-like objects (CLO) having ~ 3 nm widths, ~ 30 nm lengths, and having a high degree of order along their length. Such order implies vanishingly small bond-angle distortion. The density of the CLOs increases with increasing hydrogen dilution. At very high hydrogen dilution, TEM results show the formation of microcrystallite inclusions; it is interesting to point out that small microcrystallites are observed even in films that are deposited below the threshold under conditions that are used for making the intrinsic alloys for the highest quality cells.

Raman measurements show a continuous shift of the TO peak 475 cm⁻¹ to higher wave numbers with increasing hydrogen dilution. The results are interpreted by assigning a TO band existing at 490 cm⁻¹ that exists in all the samples but increases in magnitude with increasing hydrogen dilution. This band is inferred to be the signature of the intermediate ordered CLOs. The Raman peak associated with microcrystallites at ~515 cm⁻¹ is observed in over the edge samples.

X-ray diffraction (XRD) measurements [12] have also been used to investigate the structure of these films. A narrowing of the width of the first x-ray scattering peak is observed with increasing hydrogen dilution indicating improved intermediate range order. Even in samples that do not show any evidence of microcrystallinity, the width is narrower in hydrogen-diluted samples than in typical amorphous materials grown with no hydrogen dilution. At dilutions above the threshold, microcrystallites appear with significant narrowing of the width of the peak (3° as opposed to more than 5°).

A thickness dependence of the structure of the films was also demonstrated by these studies [13]. Films of different thicknesses grown under the same deposition conditions show improvement in intermediate range order as the thickness increases.

Similar dependence of degree of order on hydrogen dilution was reported by Koh et al. [14] using real time spectroscopic ellipsometry. A thickness versus hydrogen dilution phase diagram was proposed, and the region of the phase diagram near the phase boundary but below the onset was termed the 'protocrystalline' regime.

Cell performance

The tailing of the bands caused by the inherent disorder and the structural defects in the form of dangling and weak bonds act as recombination and trap centers, and affect the transport of carriers in a-Si alloy. Metastable defects [15] that are created on light exposure imposed further challenges on the usefulness of this material for solar cells. Stability issues forced us to use thinner cells where carriers need to move only a short distance before they reach the electrodes, and the degradation is small even when new defects are created by light exposure. To compensate for insufficient absorption of light in thin cells, a stacked-cell approach was developed where multiple thin cells of different bandgaps are stacked together. The most efficient approach has been the triple-cell design where three cells are stacked together as shown in Fig. 1.

The top cell, which captures the blue photons, uses a-Si alloy with an optical gap of ~ 1.8 eV for the intrinsic (*i*) layer. The *i* layer for the middle cell is an amorphous silicon-germanium (a-SiGe) alloy with about 10-15% Ge. The optical gap is ~ 1.6 eV, which is ideally suited for absorbing the green photons. The bottom cell captures the red and infrared photons and uses an *i* layer of a-SiGe alloy with about 40-50% Ge, corresponding to an optical gap of ~ 1.4 eV. Light



Figure 1. Schematic of triple-junction cell.

that is not absorbed in the cells gets reflected from the silver/zinc oxide (Ag/ZnO) back reflector, which is usually textured to facilitate light trapping. The cells are interconnected by the heavily doped layers that form tunnel junctions between adjacent cells.

In order to obtain the highest cell efficiency, the component cells of a triple-junction structure have to be individually optimized. The characteristics for the component cells as a function of hydrogen dilution are shown in Tables I - III. As the hydrogen dilution increases, the cell performance improves till one goes over the edge when the material becomes mixed phase and the performance drops. Since there is a concurrent drop in open-circuit voltage (V_{oc}), one can use the magnitude of V_{oc} as the indicator of amorphous to microcrystalline transition. To obtain the component cell with the highest efficiency, the hydrogen dilution is increased till V_{oc} drops. One then reduces the dilution a little bit to get the optimum performance. We should note from Table I that with hydrogen dilution large enough to take a-Si over the edge, the fill factor starts improving again. This is the microcrystalline phase with small grain-size, and this regime has received a great deal of attention for designing high efficiency cells.

Table I. J-V characteristics measured under AM1.5 illumination of a-Si alloy top cells on stainless steel with four different hydrogen dilutions.

Hydrogen Dilution	J_{sc} (mA/cm ²)	V_{oc} (V)	FF	P_{max} (mW/cm ²)
Near-optimum	10.04	1.018	0.732	7.48
Optimum	9.88	1.028	0.761	7.73
On-the-edge	9.82	0.624	0.426	2.61
Over-the-edge	8.95	0.459	0.562	2.31

Table II. J-V characteristics measured under AM1.5 illumination with a $\lambda > 530$ nm filter of a-SiGe alloy middle cells on stainless steel with four different hydrogen dilutions.

Hydrogen Dilution	J_{sc} (mA/cm ²)	V_{oc} (V)	FF	P_{max} (mW/cm ²)
Near-optimum	10.70	0.738	0.596	4.71
Optimum	10.60	0.756	0.654	5.24
On-the-edge	10.67	0.617	0.607	4.00
Over-the-edge	10.94	0.447	0.439	2.15

Table III. J-V characteristics measured under AM1.5 illumination with a $\lambda > 530$ nm filter of a-SiGe alloy bottom cells on stainless steel with four different hydrogen dilutions.

Hydrogen Dilution	J_{sc} (mA/cm ²)	V_{oc} (V)	FF	P_{max} (mW/cm ²)
Near-optimum	10.81	0.656	0.555	3.94
Optimum	10.78	0.654	0.639	4.51
On-the-edge	11.35	0.494	0.453	2.54
Over-the-edge	11.64	0.356	0.427	1.77

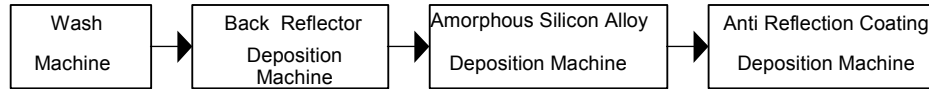


Figure 2. Schematic of the four production roll-to-roll deposition machines.

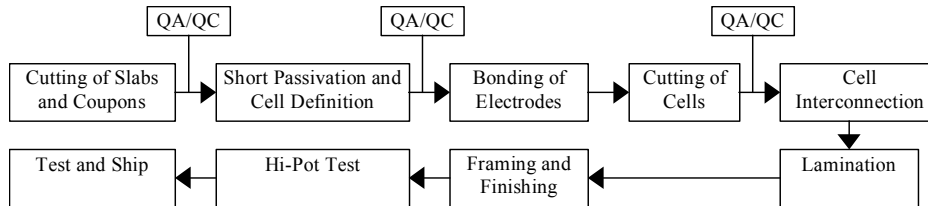


Figure 3. Semiautomated module assembly operation.

The highest cell efficiencies obtained with single- and multi-junction structures show that a stable efficiency beyond 10% can be achieved only when one uses multi-junction structure. The highest stable efficiency achieved to date is 13%. Where do we go from here? Improvement of a-SiGe alloy is still the biggest challenge. While many laboratories are actively working on it, improving the quality of the material at high deposition rate is also receiving a great deal of attention. The best material is typically grown at around 0.1 nm/sec where as a deposition rate of 0.3 nm/sec is used in production. Efficiency decreases with increasing deposition rates, and maintaining the same efficiency as the deposition rate increases can lower the cost of production significantly.

Manufacturing

Several manufacturers have been in production of a-Si alloy solar panels using either a superstrate or a substrate structure. In the superstrate structure, the carrier on which the various layers of thin films are deposited to form the solar cell serves as a window to the cells. The most common superstrate is glass, and several companies in Europe and Japan have been in production of single- and multi-junction solar panels using a monolithic laser-integrated approach [16].

In the substrate configuration, the cell is deposited on an opaque substrate and the light enters through the top anti-reflection coating layer as shown in Fig. 1. The advantage of the substrate configuration is the use of a flexible substrate that can be used in a roll-to-roll operation. We have developed a roll-to-roll automated process for manufacturing solar cells on stainless steel. Rolls of stainless steel, a mile and a half (2500 m) long, 14 in (36 cm) wide, and 5 mil (125 μm) thick, move in a continuous manner in four machines to complete the solar cell fabrication. The machines are (Fig. 2): 1) The wash machine that washes the web one roll at a time; 2) the back reflector machine that deposits the back reflector by sputtering Al and ZnO on the three rolls of washed webs at a time; 3) the triple junction amorphous silicon alloy processor that deposit the nine layers of a-Si and a-SiGe alloy layers on six rolls of back reflector coated stainless steels at a time; and 4) the anti-reflection coating machine that deposits indium tin oxide (ITO) on top of the three rolls of stainless steel at a time.

Both the transport of the web and the process parameters are computer-controlled ensuring reliable and low-cost operation. We use Al back reflector in manufacturing rather than Ag to

reduce cost. The coated web is next processed to make a variety of lightweight, flexible and rugged products. The module assembly operation consists of the following steps (Fig. 3). The finished roll of the coated web is first cut into 23.9 cm x 36 cm slabs using a semiautomated press; coupons are also cut during the same operation at preset intervals along the length of the web.

These coupons are processed off-line for QA/QC evaluation. The slabs are then processed to define cell size, passivated to remove shunts and shorts, and tested to ascertain quality. Grid wires and contact pads are next applied, and the slabs are cut into predetermined cell sizes for the various product requirements. The cells are next interconnected and the cell-block laminated to provide protection against outside atmosphere. Depending on the application, frames and junction boxes are added, and the finished modules undergo a hi-pot test and performance measurement under global AM1.5 illumination before they are shipped out.

A schematic diagram of our triple-junction cell processor is shown in Fig.4. The machine is approximately 90 m long and 3 m tall. There is a vertical central cathode and three webs are transported on each side of the cathode parallel to it at 2 feet (30 cm) a minute. Nine miles (14.5 km) of solar cells can thus be produced per run in 72 hours!

The vertical cathode and dual-side deposition system allow easy maintenance and improved gas utilization. The deposition machine has several other improved features [17]:

- The pumping system has redundancy to eliminate production interruption.
- New cathode systems provide improved deposition uniformity.
- Pinch valve between loading/unloading and deposition chambers improve turn around time.
- *In situ* performance diagnostic system provide information about the component and the triple-junction cells while the run is progressing.

The plant is now operational and is in the process of rapid scale up. QA results over the length of the runs show extremely tight tolerance in efficiency. As part of our QA procedure, we also make cells of 806 cm² area coated with a hard coat at an interval of 25 m. The average power output of these cells over about 60 runs is shown in Fig. 5. The run lengths varied from 800 to 2500 m. Again even in the initial stages of production the consistency is extremely good.

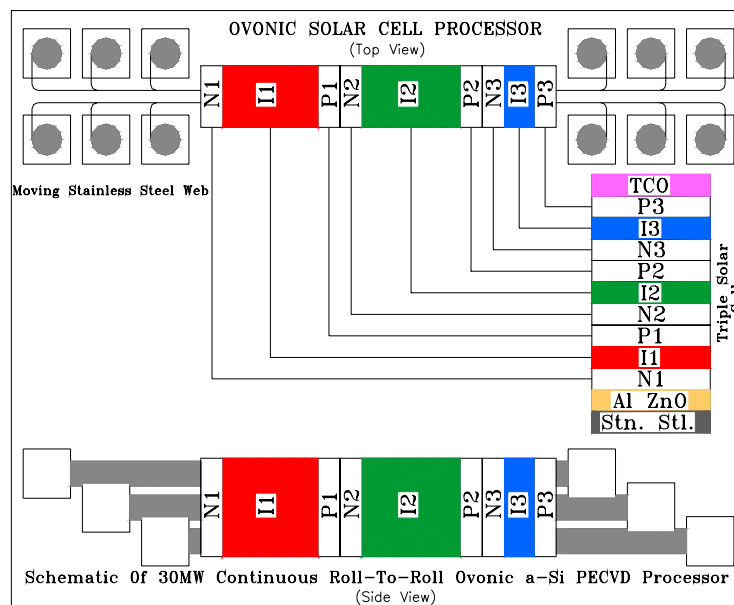


Figure 4. Amorphous silicon alloy triple-junction cell processor.

density of defects. Over the last decade, significant advances in our understanding of this material have emerged leading to achieving efficiencies comparable to those of multi-junction a-Si alloy solar cells [16]. Many different deposition methods have been used using radio frequency, very high frequency and microwave for decomposition of silane.

With increasing hydrogen dilution, the amorphous to microcrystalline transition takes place. If the dilution is further increased, the size of the grains increases, and this results in a material full of voids and grain boundaries. The highest cell efficiency, therefore, is obtained when the dilution is just above the edge [5]. Since the order improves in the growth direction, at any given dilution, the grain size increases as a function of thickness. This may result in poorer material quality for thick films. This problem is especially acute in solar cell structure where one needs thickness in excess of one μm to absorb the sunlight efficiently. In Table IV, we show the J-V characteristics of solar cells in which the thickness of the intrinsic layer was increased. The drop in fill factor with thickness can only be explained by assuming deterioration of the material quality as the thickness increases. The voltage drop with thickness also suggests that grain size is increasing.

By changing the hydrogen dilution with time, the deposition conditions can always be kept near the edge. This ensures small and uniform grain size through out the film thickness and results in improvement of efficiency. Typical results [18] with and without hydrogen dilution profiling are shown in Table V. A dramatic improvement in efficiency is observed.

Table IV. J-V characteristics of microcrystalline silicon solar cells deposited on stainless steel with different thicknesses.

Run No.	Thickness (nm)	Q (mA/cm^2)	V_{oc} (V)	FF	P_{max} (mW/cm^2)
12129	335	9.45	0.47	0.651	2.89
12125	470	10.98	0.466	0.672	3.44
12127	720	12.99	0.439	0.64	3.65
12123	1040	14.8	0.434	0.621	3.99
12128	1305	16.51	0.414	0.578	3.95
12126	1980	17.87	0.393	0.510	3.58

Table V. J-V characteristics of $\mu\text{c-Si:H}$ single-junction solar cells. Sample 14554 is the baseline cell, sample 14559 is with a 20% thicker intrinsic layer than the baseline, and sample 14660 is with a hydrogen dilution profiled intrinsic layer.

Sample No.	J_{sc} (mA/cm^2)	V_{oc} (V)	FF	Eff (%)
14554	22.58	0.495	0.603	6.74
14559	21.48	0.482	0.632	6.54
14660	25.15	0.502	0.663	8.37

We have previously reported an initial active-area efficiency of 13% using a double-junction a-Si/ $\mu\text{c Si}$ structure. The stable efficiency was 11.2%. The device did not incorporate hydrogen dilution profiling in the bottom cell; with the incorporation of hydrogen dilution profiling we have now achieved 13.5%. Other laboratories have reported initial efficiencies in the range of 13 to 14.7% [16].

While the above results are very promising, there are two major challenges to solve before large-scale commercialization takes place. The highest efficiency cells are made by glow discharge deposition using very high frequency or radio frequency at high pressure. Control of uniformity in deposition under these conditions is a major challenge. The deposition time is also long since the layers are thicker than one μm . High efficiency cells must be made at deposition rates exceeding 1.5 nm/sec to make the device economically viable.

While several manufacturers have been aggressively pursuing research in this area, Kaneka Corporation [16] has already started limited production of tandem solar panels using a-Si and microcrystalline silicon. Trial productions show initial module efficiencies in the range of 11%. This could lead to stable efficiencies in the 9 to 10% range.

NEW APPLICATIONS

There is an emerging need for lightweight solar arrays on flexible substrates for satellite and airship applications. Future spacecrafts need large arrays (30-50 kW) that can be stowed during launching, and rolled out in the orbit. There is also a need by the U.S. Department of Defense for giant airships to be stationary in the stratosphere for communication and reconnaissance purpose. The development of rugged thin film solar cells with high specific power on lightweight flexible substrates is an enabling technology for such applications. In many cases, low cost is also an important criterion. Current high-efficiency crystalline space solar cells cannot satisfy the three key requirements of (1) high specific power, (2) mechanically rugged and stowable properties, and (3) low cost. Typical specific power for the crystalline cells is <100 W/kg. The panels are fragile and need a heavy and fragile cover glass. The solar array cost is high, at \sim \\$500-\\$2000/watt. In contrast, United Solar's a-Si triple-junction solar cells on flexible substrates address all these issues. The specific power is high since (1) the cells are very thin and (2) the substrates are flexible and lightweight. The cells are rugged mechanically since there is no breakable part. The cost is potentially an order of magnitude lower.

In addition to the high specific power, mechanical ruggedness, and low cost that United Solar's triple-junction solar cells can offer, certain space qualification tests have also shown promising results [1]. For example, the temperature coefficient for high efficiency triple-junction a-Si alloy cells has been found to be between -0.2 and -0.3% / $^{\circ}\text{C}$, which is superior to crystalline Si devices for high temperature operation. In addition, United Solar's triple-junction cells on SS have been subjected to proton and electron irradiations of various energies and fluences. It has been found that defects that are created by irradiation can be annealed out and cell efficiency restored at the prevailing temperature of ~ 70 $^{\circ}\text{C}$ in orbit. Furthermore, a-Si alloy triple-junction solar cells bonded to an appropriate substrate structure have been subjected to $+150$ $^{\circ}\text{C}$ to -110 $^{\circ}\text{C}$ thermal cycles at 80 $^{\circ}\text{C}$ / min. No change in cell performance was detected.

The AM0 spectrum is much richer in the blue wavelength region than the AM1.5 spectrum prevalent on the earth. The thickness and band gap of the component cells are re-optimized for the AM0 spectrum. We have demonstrated a total area beginning-of-life efficiency of 12% measured by NASA.

Two different approaches have been taken for substrate selection. In the first approach, where SS is used, the roll-to-roll production technology has been used to make the solar cells, and the cells are fabricated using the terrestrial production technology, as discussed earlier. The substrate is, however, less than one mil thick, and the cells are optimized for the AM0 spectrum. Typical beginning-of-life efficiency for the cells from the production line is 8.5%. The corresponding value for R & D cells with an area of 460 cm² is 9.5%, as confirmed by NASA Glenn Research Center.

In the second approach, we use a one-mil-thick polyimide substrate. The cells on polyimide are at an initial stage of development, but have already shown promising results. NASA Glenn has measured cells with 412 cm² area at 9% beginning-of-life efficiency.

The advantage of using the SS substrate is that the production technology exists, and we can readily meet the volume demand. The specific power for a triple-junction cell on thin SS has exceeded 350 W/kg. Future work is aimed at increasing the specific power to over 500 W/kg. For cells on polyimide, the advantage is higher specific power. We have achieved a specific power exceeding 1250 W/kg using R&D machines. We are now developing the manufacturing technology for producing such cells using polyimide bonded/cast on stainless steel. This allows use of the conventional roll-to-roll process for producing such cells.

CONCLUSION

Thin-film silicon made using hydrogen dilution near the edge of amorphous to microcrystalline transition has emerged as a viable candidate for large-scale manufacture of solar cells. The material below the edge has received more attention, and manufacturing plants are in operation producing a variety of products using a-Si alloy technology. Light-induced degradation limits the highest efficiency obtained with this material. Although many innovative methods are being used to improve the efficiency further, an alternate method is to use the material grown above the edge (i.e. microcrystalline silicon). Impressive progress has been made in this field as well, and thin-film silicon solar cells are expected to play a major role in the photovoltaic market. New applications in space and stratosphere are enhancing the opportunities for these products in those premium markets.

ACKNOWLEDGMENTS

The author is grateful to J. Yang, A. Banerjee, K. Lord, B. Yan, P. Nath, K. Hoffman, and J. Call for discussion and collaboration, and S. Sundquist for preparation of the paper. The work has been supported in part by NREL under subcontracts ZAK-8-17619-09 and ZDJ-2-30630-19.

REFERENCES

1. J. Yang, A. Banerjee, and S. Guha, *Solar Energy Mat. & Solar Cells*, **78**, 597 (2003).
2. A. V. Shah, J. Meier, E. Vallat-Sauvain, J. Wyrsh, U. Kroll, C. Droz, and U. Graf, *Solar Energy Mat. & Sol. Cells*, **78**, 459 (2003).
3. S. Guha, K. L. Narasimhan, and S. M. Pietruszko, *J. Appl. Phys.* **52**, 859 (1981).
4. D. V. Tsu, B. S. Chao, S. R. Ovshinsky, S. Guha, and J. Yang, *Appl. Phys. Lett.*, **71**, 1317 (1997).

5. O. Vetterl, R. Carius, L. Houben, O. Kluth, A. Lambertz, A. Muck, B. Rech, and H. Wagner, *Solar Energy Mat. & Sol. Cells*, **62**, 97 (2000)
6. A. Gallagher, *J. Appl. Phys.*, **63**, 2406 (1988).
7. A. Matsuda, 25th IEEE PVSC, 1029, (1996).
8. A. Matsuda, *J. Non-Cryst. Solids*, **59-60**, 767 (1983).
9. C. C. Tsai, G. B. Anderson, R. Thomson, and B Wacker, *J. Non-Cryst. Solids*, **114**, 151 (1989).
10. N. Shibata, K. Fukuda, H. Ohtoshi, J. Hanna, S. Oda, and I Shimizu, *Mat. Res. Soc Symp. Proc.*, **95**, 225 (1987).
11. S. Sriraman, S. Agarwal, E. S. Aydil and D. Maroudas, *Nature*, **418**, 62 (2002).
12. D. L. Williamson, *Mat. Res. Soc. Symp. Proc.* **557**, 251 (1999).
13. S. Guha, J. Yang, D. L. Williamson, Y. Lubianiker, J. D. Cohen and A.H. Mahan, *Appl. Phys. Lett.* **74**, 1860 (1999).
14. J. H. Koh, Y. Lee, H. Fujiwara, C. R. Wronski, and R. W. Collins, *Appl. Phys. Lett.*, **73**, 1526 (1998).
15. D. L. Staebler and C. R. Wronski, *Appl. Phys. Lett.* **31**, 292 (1977).
16. Y. Tawada, H. Yamagishi, and K. Yamamoto, *Solar Energy Mat. & Solar Cells*, **78**, 647 (2003).
17. M. Izu and T. Ellison, *Solar Energy Mat. & Solar Cells*, **78**, 613 (2003).
18. B. Yan, G. Yue, J. Yang, S. Guha, D. L. Williamson, D. Han, and C. S. Jiang, (to be published).